scientific reports

Check for updates

OPEN

An *Andrias davidianus* derived composite hydrogel with enhanced antibacterial and bone repair properties for osteomyelitis treatment

Chong Yin[1,2,6], Meng Deng[1,2,6], Jinshu Yu[1,2,6], Yonghao Chen[1,2], Kaiyuan Zheng[3], Yi Huang[1,2], Xudong Deng[4], Ye Tian[4], Yuwen Ma[1,2], Beilei Zeng[5], Xiaolan Guo[1,2]✉ & Bin Guo[1,2]✉

Effective antibacterial therapy while accelerating the repair of bone defects is crucial for the treatment of osteomyelitis. Inspired by the protective mechanism of *Andrias davidianus*, we constructed an antibacterial hydrogel scaffold with excellent rigidity and long-term slow-release activity. While retaining the toughness of the skin secretion of *Andrias davidianus* (SSAD), the rigidity of the hydrogel material is increased by incorporating hydroxyapatite to meet the demands of bone-defect-filling materials. It also exerted antibacterial effects via the slow-release of vancomycin from local osteomyelitis lesions. Notably, the hydrogel can also carry a high stable recombinant miR-214-3p inhibitor (MSA-anti214). By the delivery of nano vector polyvinylamine, the long-term slow-release of MSA-anti214 is achieved to promote bone repair, making this composite hydrogel a potential SSAD-based osteomyelitis alleviator (SOA). In vitro and *vivo* results verified that the SOA effectively eliminated *Staphylococcus aureus* and repaired bone defects, ultimately mitigating the progression of osteomyelitis. This composite hydrogel extends the economic application prospects of *A. davidianus* and has provided new insights for the treatment of osteomyelitis. The study also explored new insights for the bone filling materials of bone defection and other skeletal system diseases.

Keywords *Andrias davidianus*, Osteomyelitis, Natural polymer-based hydrogels, Nucleic acid drugs, Bone-defect-filling materials

Osteomyelitis is a chronic disease that closely associated with open fractures and joint replacement[1–3]. *S. aureus*-induced osteomyelitis can lead to prolonged bone pain, osteonecrosis, and even amputation or fatal sepsis[4,5]. Currently, the typical clinical treatment modalities include thorough debridement and long-term systemic antibiotic therapy. However, traditional long-term antibiotics and the presence of the bone marrow–blood barrier can have severe impacts, such as low local drug concentrations or drug-resistance of bacteria[6,7].

As a treatment for osteomyelitis, bone-defect-filling materials have attracted the attention of clinicians and scholars owing to their excellent biocompatibility and the local delivery of antibiotics. The reported bone-defect-filling materials mainly include polymethylmethacrylate (PMMA)[8], calcium phosphate[9], hydroxyapatite (HA)[10], collagen implants[11], and bioactive glass[12]. PMMA has excellent mechanical and injectable properties and is the most widely used bone-defect-filling material. For instance, Tan et al.[13] synthesized 26% chitosan-loaded PMMA bone cement, which effectively inhibited *Staphylococcus* on the surface of the bone cement. Nonetheless, owing to the nonbiodegradability, burst effect, and heat production of PMMA, natural polymer-based hydrogels have received increasing attention[14].

[1]Department of Clinical Laboratory, Affiliated Hospital of North Sichuan Medical College, Nanchong 637000, People's Republic of China. [2]School of Laboratory Medicine, Translational Medicine Research Center, North Sichuan Medical College, Nanchong 637000, People's Republic of China. [3]Department of Rehabilitation Medicine, Affiliated Hospital of North Sichuan Medical College, Nanchong 637000, People's Republic of China. [4]Key Lab for Space Biosciences and Biotechnology, School of Life Sciences, Northwestern Polytechnical University, Xi'an 710072, Shaanxi, People's Republic of China. [5]Department of Oncology, Affiliated Hospital of North Sichuan Medical College, Nanchong 637000, People's Republic of China. [6]Chong Yin, Meng Deng and Jinshu Yu contributed equally to this work. ✉email: zhzxguo@nsmc.edu.cn; guobin@nsmc.edu.cn

Natural polymer-based hydrogels have emerged as favorable bone-defect-filling materials because of their intrinsic biocompatibility, degradability, and potential slow-release effects[15–18]. For instance, Yan et al.[19] fabricated a functionalized silk fibroin hydrogel that effectively promoted bone defect repair rate. Nilforoushzadeh et al.[20] reported that a composite hydrogel of calcium alginate and fibroblast cell-seeded collagen scaffolds effectively treated diabetic foot ulcer-related osteomyelitis. Nevertheless, these natural polymer-based hydrogels are still limited in their use as bone-defect-filling materials because of their expensive and cumbersome preparation[20,21]. Thus, it is imperative to develop natural bone-defect-filling materials with low cost and convenient manufacturing.

As an economically valuable amphibian, *Andrias davidianus* is widely cultivated in Shaanxi, China. Its skin secretes a protective mucus (skin secretion of *Andrias davidianus*, SSAD), which is a glycoprotein hydrogel consisting of hydrogen and disulfide bonds that is cost-effective and easy to extract and prepare[22]. Zhang et al.[22–25] showed that SSAD has exceptional toughness, biocompatibility, and local drug delivery ability, and therefore, has drawn extensive research interest in the areas of hemostasis, infection treatment, and wound repair.

However, as a bone-defect-filling material, SSAD has limited rigidity, making it difficult to provide effective mechanical support for bone defects. Previous studies have indicated that HA, a component of natural bone tissue, is widely employed as an ideal implant material for bone defection[26–28]. Hence, the introduction of HA was expected to endow the SSAD/HA hydrogel with excellent rigidity and osteogenic properties to support bone defects and facilitate osteomyelitis recovery. This inexpensive and highly rigid hydrogel material shows great potential for the clinical treatment of osteomyelitis.

In addition, previous studies have shown that the majority of natural polymer-based hydrogels are based on their inherent properties or carry small-molecule drugs to help treat bone defects[29–31]. Compared to small-molecule drugs, nucleic acid drugs have the unique advantages of high targeting and specificity; however, efficient long-term delivery has always been a bottleneck in nucleic acid drug research[32,33]. According to a previous study, polyvinylamine (PVAm), an emerging nucleic acid delivery nanocarrier can efficiently transfect multiple RNAs both in vivo and in vitro[34]. Meanwhile, the therapeutic inhibition of miR-214 using antagomir-214 efficiently enhanced bone formation[35]. Based on this, we synthesized a stable osteogenic recombinant antagomir-214 (MSA-anti214) using novel recombinant RNA technology, which also exhibited higher biological activity and stability than normal antagomir-214[36,37]. The subsequent combination of MSA-anti214 and PVAm may significantly enhance transfection efficiency. Ultimately, it promotes efficiently the rate of bone formation and the repair of bone defects[34].

Inspired by the secretion of skin mucus by *Andrias davidianus* to resist external stimuli, we constructed an inexpensive antibacterial hydrogel with excellent biocompatibility and rigidity (Fig. 1). First, HA was embedded in SSAD to form a highly rigid SSAD/HA antibacterial hydrogel carrier. To treat osteomyelitis, PVAm-loaded MSA-anti214 (PM214) and vancomycin (Van), which is highly efficient against *S. aureus*, were encapsulated in SSAD/HA to synthesize an SSAD-based osteomyelitis alleviator (SOA). The SOA was then implanted locally into the infection site, and the osteogenic activators PM214 and Van were released in a long-term manner from SSAD/HA. In this study, we propose a simple yet effective strategy for fabricating SOA to achieve greatly enhanced bacteriostasis and bone regeneration. This may provide novel ideas for nucleic acid drug delivery for the treatment of osteomyelitis, and explore new insights for the bone filling materials of other skeletal system diseases.

Results

Characterization of SOA

SSAD was collected, freeze-dried, and ground into a powder. The SSAD powder was then mixed with deionized water to form a hydrogel. The SSAD hydrogel had a water content of 75% (Figure S1A, Supporting Information). The hydrogel was doped with different proportions of HA during its preparation. Scanning electron microscopy (SEM) observation showed that the pure SSAD hydrogel exhibited regular microstructures. The microstructure of the SSAD/HA hydrogel at a 1:1 ratio did not change significantly compared to that of pure SSAD, and HA was evenly distributed on the hydrogel, confirming that the addition of HA did not affect the microstructure of SSAD at this ratio. However, at a ratio of 2:1, the pore size of the SSAD/HA hydrogel SEM image decreased. At a ratio of 1:2, there was abundant HA powder in the pores, and the pore walls were clearly thinner. The hydrogel displayed a fragmented structure of various sizes at a ratio of 1:3 (Fig. 2A, C). This revealed that the structure of the SSAD/HA hydrogel collapsed gradually as the proportion of HA increased, and the HA powder could no longer be wrapped. Therefore, a 1:1 hydrogel ratio was used for subsequent experiments. Energy-dispersive spectroscopy (EDS) was employed to identify the elements in SSAD, including C, N, O, S, Cl, and K (Fig. 2D). Meanwhile, EDS mapping showed that HA was evenly distributed in the hydrogel (Fig. 2B).

To provide the hydrogel with an efficient nucleic acid (NA)-delivery capability, we introduced PVAm, a delivery vector for efficient RNA delivery. The water content of the SSAD hydrogel containing PVAm was 74%, which is approximate to the water content of the SSAD hydrogel alone (Figure S1A, Supporting Information). Fourier-transform infrared spectrometry (FTIR) showed that the addition of PVAm did not change the chemical groups compared with pure SSAD (Fig. 2E). Generally, swelling can significantly damage the network structure and degrade the mechanical properties of hydrogels. As shown in Figure S1C (Supporting Information), the swelling ratio of the hydrogel showed almost no change after the addition of HA and remained stable. On the 14th day, the SSAD/HA hydrogel degraded to 15.1% of its original size, through collagenase II (100 U mL^{-1}) treatment (Figure S1D, Supporting Information).

Furthermore, the storage modulus (G′) of all hydrogels was higher than the loss modulus (G′′), indicating excellent stability and elasticity of the hydrogels. As shown in Fig. 2F, the G′ of the SSAD hydrogel was 1,950.92 ± 26.53 Pa, which increased to 4,995.56 ± 383.02 Pa after the addition of HA. Meanwhile, the G′′

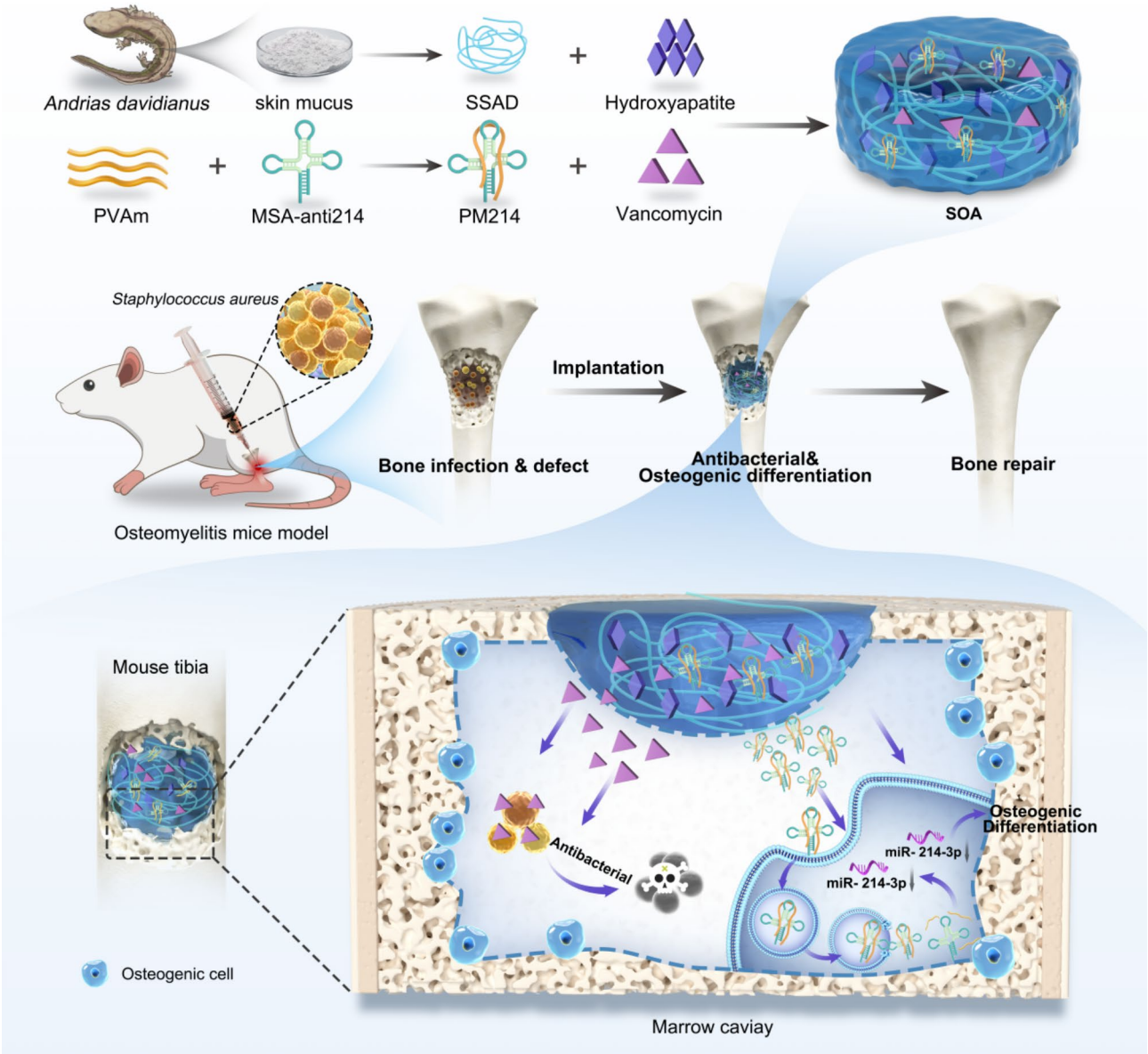

Fig. 1. Schematic diagram of the *Andrias davidianus*-derived natural polymer-based hydrogel to antibacterial and bone repair through long-term release of vancomycin and MSA-anti214. This graphic is licensed under CC BY-SA 4.0 (https://creativecommons.org/licenses/by/4.0/).

increased from 241.02 ± 18.04 Pa for SSAD to 880.57 ± 42.21 Pa for the SSAD/HA hydrogel. This suggested that the rigidity and elasticity of the SSAD hydrogel were remarkably enhanced by the addition of HA.

Deionized water, PVAm, and PVAm/NA were used separately to form hydrogels with SSAD, and their rheological properties were measured. After adding PVAm, the G′ and G′′ values of the hydrogel barely changed (Figure S1B, Supporting Information). This indicated that the addition of PVAm did not affect the rheological properties of the SSAD hydrogel. HA was then introduced and demonstrated no significant effects among the three different hydrogels (Fig. 2G).

Moreover, the slow-release capability of the SSAD/HA hydrogel on small-molecule drugs and nucleic acid drugs was analyzed. Relative quantitative analysis of slow-release properties was performed using the fluorescent dye rhodamine B. SSAD/HA was found to sustainably release rhodamine B for up to 28 d (Fig. 2H). Next, SSAD/HA was used to carry nucleic acid FAM-NC (fluorescein-labeled negative control) and FAM-NC wrapped in PVAm. The results showed (Fig. 2I) that the released FAM-NC was higher with the absence of PVAm in the first 4 days, while after 4 days, the released FAM-NC level became more stable through the addition of PVAm, and with sufficient fluorescence intensity remaining until the 28th day. This finding suggests that the SSAD/HA hydrogel with PVAm can stabilize and release nucleic acids sustainably for a long time, which raises the likelihood of the long-term treatment of bone defects with nucleic acid drugs.

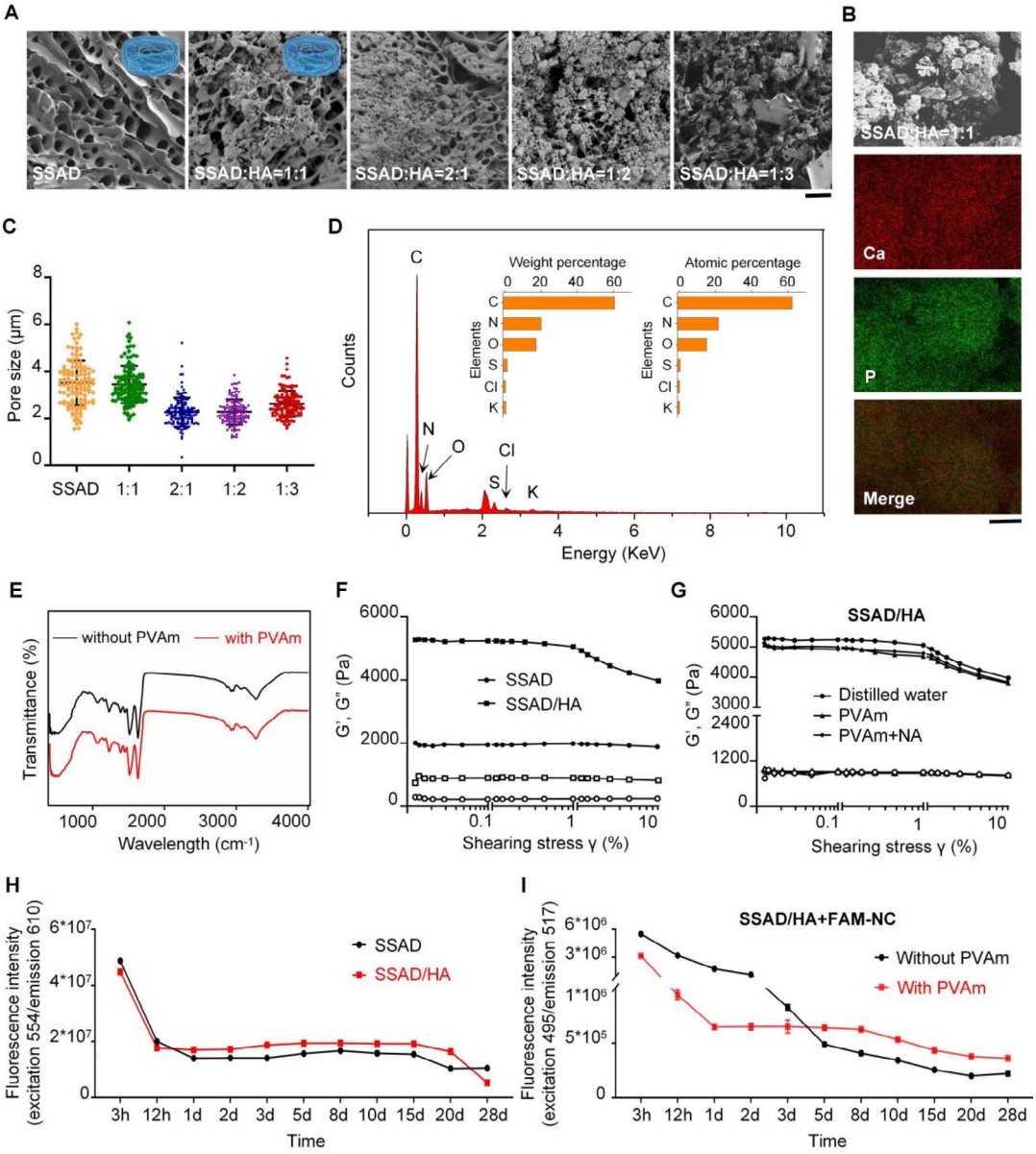

Fig. 2. Characterization of SSAD and SSAD/HA hydrogels. **A** Scanning electron microscope (SEM) images of the skin secretion of *Andrias davidianus* (SSAD) and SSAD/hydroxyapatite (HA) hydrogels at different ratios. Scale bar, 10 μm. **B** Energy-dispersive spectroscopy mapping of the SSAD/HA hydrogel. Scale bar, 5 μm. (C) Pore size distribution of the corresponding hydrogels in (**A**) based on random measurements of at least 100 pores. **D** Energy dispersive spectroscopy analysis of the SSAD hydrogel, including C, N, O, S, Cl, and K. **E** Fourier-transform infrared spectrometry (FTIR) spectra of the SSAD hydrogel with or without polyvinylamine (PVAm). **F** Rheological behavior of SSAD and SSAD/HA hydrogels. Hollow indicates G". Solid indicates G′. **G** Rheological behavior of the SSAD/HA hydrogels formed by deionized water, PVAm, and PVAm/NA separately. The deionized water group data are consistent with the SSAD/HA group data in Fig. 1F. Hollow indicates G". Solid indicates G′. **H** Validation of the slow-release of small-molecule drugs by SSAD and SSAD/HA hydrogels. **I** Verification of the slow-release of nucleic acids (FAM-NC) by SSAD/HA hydrogels in the presence or absence of PVAm. All quantitative data are presented as mean values ± standard deviation ($n = 3$, * $p < 0.05$, ** $p < 0.01$, *** $p < 0.001$, ns: no significance).

Antibacterial properties of the SOA in vitro

The optimal Van concentration for inhibiting *S. aureus* was evaluated as 100 mg mL^{-1} (Figure S3A, B, Supporting Information). First, the antibacterial and osteogenic properties of the hydrogels were evaluated according to the schematic of Fig. 3A. The colony diagram (Fig. 3C, E) shows that the number of colonies in the SSAD group decreased by 67.5%, and SSAD/HA hydrogel (+HA hydrogel) group displayed a 75.2% reduction compared to PBS ($p < 0.01$). For the SSAD/HA + Van hydrogel (+Van hydrogel), the number of colonies reduced by 98.6%, indicating significant antibacterial activity in the presence of Van. The antibacterial activity was similar to pure Van solution (100%). These findings suggest that the hydrogel nearly completely eliminated environmental *S. aureus* through the addition of Van. Similarly, the +Van hydrogel had a remarkable antibacterial ring compared to the SSAD group (Figure S3C, D, Supporting Information).

Slow-release antibacterial properties of the SOA in vitro

To treat osteomyelitis, an effective antibiotic concentration must be retained for a long time. It was confirmed that the +HA hydrogel (SSAD/HA hydrogel) was able to slowly release the small-molecule rhodamine B (Fig. 2H). Hence, the slow-release of Van by the +HA hydrogel was further explored. As shown in Fig. 3D, F, it displayed noticeable antibacterial activity within 14 days, with bacterial survival decreased to 30.6% by day 20. These findings revealed that the +HA hydrogel was able to slowly release Van in a stable manner over a period of 14 d. Thus, it was confirmed that the +Van hydrogel had effective antibacterial properties in vitro and could successfully suppress *S. aureus* over a long period.

Osteogenic properties of the SOA in vitro

To further demonstrate the ability of this hydrogel to carry nucleic acids, nucleic acid delivery system PVAm was used to combine two miR-214-3p inhibitors, separately, antagomir-214 and recombinant antagomir-214 (MSA-anti214), to form PVAm/antagomir-214 (P214) or PVAm/MSA-anti214 (PM214). Whereafter, these two compounds were wrapped in +Van hydrogel to synthesize the SSAD/HA + Van + P214 and SSAD/HA + Van + PM214 hydrogel, with antagomir-NC and recombinant scaffold ($tRNA^{Met}$-fused Sephadex aptamer, MSA) as controls. Human mesenchymal stem cells (hMSCs) treated with SSAD/HA + Van + P214 (+P214) or SSAD/HA + Van + PM214 (SOA) hydrogel showed no significant change in cell activity (Fig. 3B). The hemolysis assay also showed that no hemolysis occurred through hydrogel treatment (Figure S2A-B, Supporting Information). The cell cycle analysis and cell adhesion analysis showed no alteration to the cell phase percentage in all hydrogel treated cells, and hMSC could normally adhere on the surface of SOA (Figure S2C-D, Supporting Information). All results indicate favorable biocompatibility of the hydrogel, which is a prerequisite for a bone-defect-filling material.

hMSC osteogenic differentiation through hydrogel treatment was also investigated. *Alp* (alkaline phosphatase) and *Runx2* (runt-related transcription factor 2) expression levels were up-regulated by 54.6% ($p < 0.05$) and 48.1% ($p < 0.05$), respectively, after treated with +P214 hydrogel. *Alp* and *Runx2* levels were up-regulated by 61.9% ($p < 0.01$) and 50% ($p < 0.01$) respectively, in hMSCs treated with the SOA hydrogel (Fig. 3H). Alkaline phosphatase activity and mineralized nodules were also significantly increased (Fig. 3G). These results showed that the hydrogels with miR-214-3p inhibitors promoted osteogenic differentiation and that the SSAD/HA + Van + PVAm hydrogel could efficiently and safely carry nucleic acids to regulate osteogenic differentiation.

Continuously osteogenic properties of the SOA in vitro

RT-PCR was performed to estimate the nucleic acid slow release of the hydrogel to inhibit miR-214-3p in cells. The results revealed that the inhibitory effect of +P214 on miR-214-3p in hMSCs began to diminish at day 4, with no significant inhibitory effect at day 7 (Fig. 4A, $p > 0.05$). However, the SOA still had a significant inhibitory effect on miR-214-3p at 28 d (Fig. 4B, $p < 0.05$), implying that MSA-anti214 was more stable and had a higher potency than antagomir-214. The SSAD/HA + Van + PVAm hydrogel provided the long-term slow-release of MSA-anti214 and inhibited miR-214-3p.

We additionally compared the nucleic acid slow release effect of SOA and other hydrogels including Hyaluronic acid Methacryloyl (HAMA) and Gelatin Methacryloyl (GelMA). SOA presented a similar slow release effect as other hydrogels (Figure S4, Supporting Information).

Subsequently, we verified the potency of +P214 and the SOA for the long-term regulation of cell differentiation. The results showed that treating hMSCs with hydrogels significantly augmented ALP activity and mineralized nodule formation at 14 d. However, on the 28th day, ALP activity and mineralized nodules increased only in the SOA treatment group, with no effect in the +P214 group (Fig. 4E and S5A, Supporting Information). In addition, the mRNA expression levels of *Alp* and *Runx2* in hMSCs treated with +P214 returned to normal at 28 d, while SOA still had a significant promoting effect at 28 d (Fig. 4C–D and S5B–C, Supporting Information, $p < 0.01$). The results provided evidence that the SSAD/HA hydrogels were capable of the long-term slow-release of MSA-anti214 and subsequently, promoted osteogenic differentiation.

Seroprotective effect of the SOA

Nucleic acid drugs are easily degraded because of their poor stability and the presence of nucleases in the serum[38]. To further elucidate the protective effect of the SSAD/HA + Van + PVAm hydrogel on nucleic acids, the hydrogels carrying antagomir-214 or MSA-anti214 were treated with fetal bovine serum, and miR-214-3p inhibition effect was tested. As Fig. 4F–G shows, the inhibition of miR-214-3p was maintained for 4 days in the +P214 group. While in the SOA group, miR-214-3p inhibitory effect was still significant at 14 d ($p < 0.05$). This indicated that MSA-anti214, a biosynthetic RNA inhibitor, was relatively stable and less degradable than antagomir-214[39].

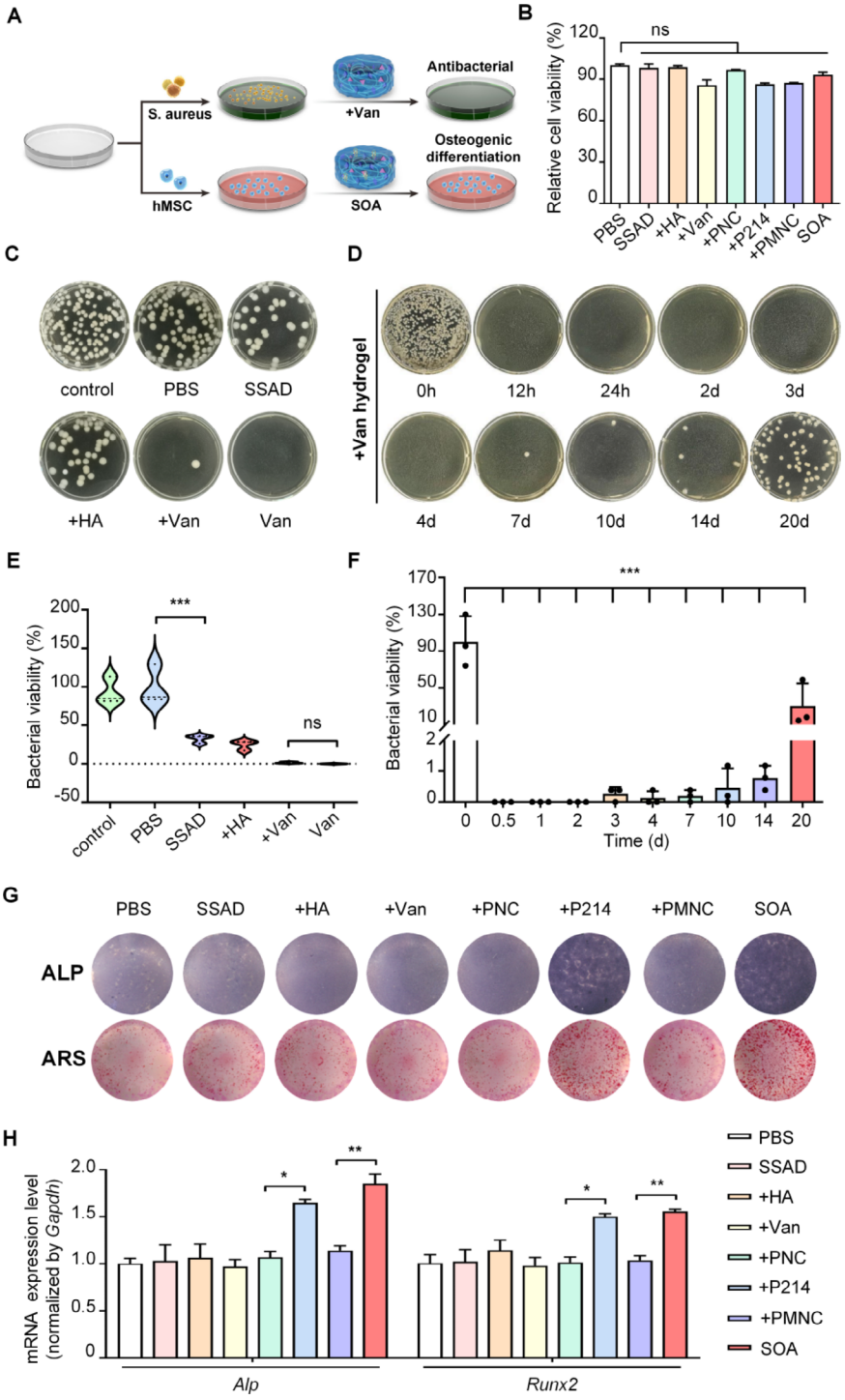

Fig. 3. Investigation of the antibacterial and osteogenic properties of the SOA hydrogel in vitro. **A** General schematic illustration of antibacterial and osteogenic studies. **B** Cytocompatibility of the SSAD-based osteomyelitis alleviator (SOA) detected using the MTT assay. SSAD: SSAD hydrogel; +HA: SSAD/HA hydrogel; +Van: SSAD/HA + Van hydrogel; +PNC: SSAD/HA + Van + PVAm/antagomir-NC hydrogel; +P214: SSAD/HA + Van + PVAm/antagomir-214 hydrogel; +PMNC: SSAD/HA + Van + PVAm/MSA hydrogel; SOA: SSAD/HA + Van + PVAm/MSA-anti214 hydrogel. **C** Images of the spread plate method. **D** Validation of the long-term antibacterial activity of the + Van hydrogel. **E** Quantification of the results in (**C**). **F** Quantification of the results in (**D**). **G** Representative images of alkaline phosphatase (ALP) staining and alizarin red staining (ARS) of human mesenchymal stem cells (hMSCs) after treatment with each hydrogel component. **H***Alp* and *Runx2* expression levels in hMSCs treated with each hydrogel component as detected by real-time polymerase chain reaction. All quantitative data are presented as mean values ± standard deviation ($n = 3$, * $p < 0.05$, ** $p < 0.01$, *** $p < 0.001$, ns: no significance).

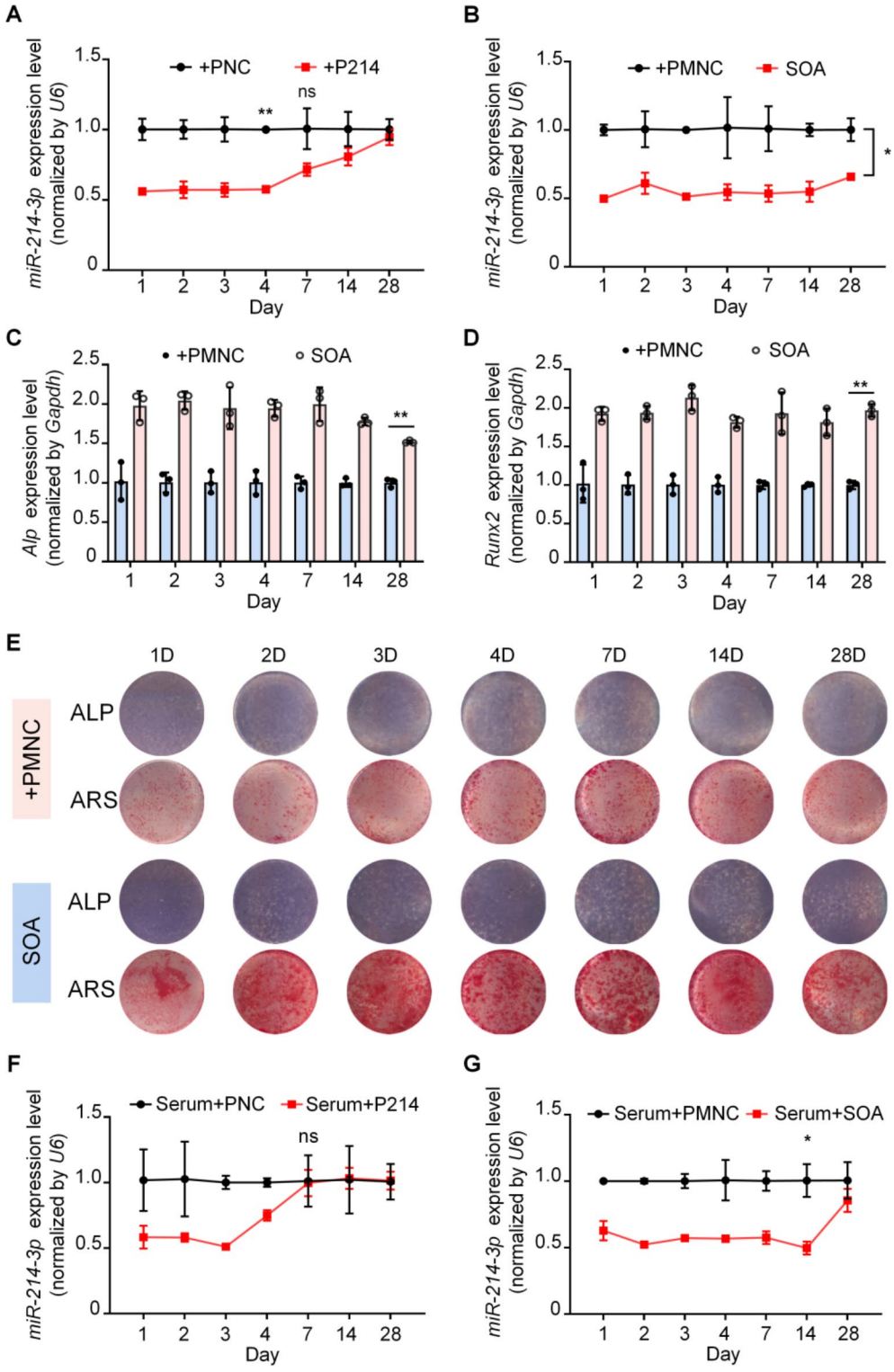

Fig. 4. The SOA hydrogel promoted osteogenic differentiation via the slow-release MSA-anti214 in vitro. miR-214-3p expression levels in hMSCs treated with **A** + P214 hydrogel and **B** the SOA separately at the specified intervals (compared with the + PNC/+PMNC hydrogel). **C***Alp* and **D***Runx2* expression levels in hMSCs treated with the SOA hydrogel. **E** ALP and alizarin red staining of hMSCs treated long-term with the SOA hydrogel compared to those treated with the + PMNC hydrogel. ALP: results of ALP staining; ARS: results of alizarin red staining. **F**–**G** miR-214-3p expression levels in hMSCs after treated with serum-pretreated + P214 (Serum + P214) and SOA (Serum + SOA) hydrogels at the specified intervals. All quantitative data are presented as mean values ± standard deviation ($n = 3$, * $p < 0.05$, ** $p < 0.01$, *** $p < 0.001$, ns: no significance).

Meanwhile, the regulatory effects of serum-treated + P214 and SOA on osteogenic differentiation were also detected. As shown in Figure S6(Supporting Information), SOA maintained osteogenic effect on day 28, whereas there was no significant effect in the + P214 group at 14 d. These data suggest that, in the presence of nucleases, the SOA can retain the long-term release of nucleic acid drugs, and showed the potential of treating osteomyelitis.

Antibacterial properties of the SOA in osteomyelitis mice

An in vivo mouse tibial infection model was established to investigate the therapeutic efficacy of SOA against osteomyelitis (Fig. 5A). As shown in Fig. 5B–C, the inflammatory factor C-reactive protein (CRP) levels in the *S. aureus* group were significantly elevated compared to those in the sham group, but procalcitonin (PCT) levels were not affected. This is because PCT levels do not typically change in response to a local infection, but they dramatically increase once sepsis occurs. The + HA hydrogel carrying Van and PVAm/MSA-anti214 was implanted into the marrow cavity of the tibia to assess its biological safety and therapeutic efficacy against osteomyelitis. Blood biochemical markers in mice, such as aspartate aminotransferase (AST), alanine aminotransferase (ALT), blood urea nitrogen (BUN), and creatinine (Cr), showed no significant changes after SOA treatment (Figure S7A–D, Supporting Information). No apparent histological morphology or pathological changes were found on SOA treated organs including heart, liver, spleen, lung, and kidney (Figure S7E, Supporting Information). These results revealed that the SOA implanted into the bone marrow cavity had no apparent toxicity or side effects in mice, confirming its excellent biocompatibility in vivo.

The antibacterial activity of the SOA against *S. aureus* in osteomyelitis lesions was also evaluated. After implantation for 4 weeks, tibial bone marrow was harvested and the bacterial number in the bone marrow was determined using consecutive dilutions and the spread plate method on soybean agar plates. The colony diagram and semi-quantitative analysis (Fig. 5D–E) showed that the SOA completely inhibited *S. aureus* colony growth. Moreover, immunohistochemical (IHC) staining results were generally consistent with the colony diagram, and the expression levels of the inflammatory factors CD3 and CD68 were significantly reduced in the SOA group (Fig. 5F–H, Figure S8, Supporting Information). These results indicated that the SOA can dramatically eradicate *S. aureus* and alleviate inflammation in osteomyelitis in mice.

Bone defect repair properties of the SOA in osteomyelitis mice

The pharmacokinetics of MSA-anti214 released by SOA showed that miR-214-3p level decreased in tibia until 14 d, with no significant changes in other organs (Figure S9, Supporting Information). Confirming the continuous suppression of miR-214-3p expression defined only in tibia.

Subsequently, bone histomorphometric analyses were performed to investigate bone repair in osteomyelitis mice treated with the SOA. The mineral apposition rate (MAR) and bone formation rate (BFR/MS) of SOA treatment in the tibial trabecular bone were increased by 71.6% and 68.8%, respectively (Fig. 6A–D; $p < 0.001$). Meanwhile, microCT analysis showed the implantation of SOA hydrogel significantly enhanced bone mass, bone mineral density (BMD), bone volume to tissue volume (BV/TV) and bone mineral content (BMC) (Fig. 6E–H). Moreover, SOA increased the expression level of OCN (an essential biomarker of bone formation), and Masson's/Goldner's trichrome staining showed new bone was formed in SOA group, with only collagen fibers growth found in other groups (Fig. 7A–D). All these results suggested that SOA could promote mice bone formation and rescue bone defects of osteomyelitis.

Discussion

Osteomyelitis has a tremendous impact on a patient's life and work because of its stubborn nature and long treatment period. In recent years, multitudinous bone-defect-filling materials have been employed to deliver drugs locally for the treatment of osteomyelitis, greatly minimizing the side effects arising from high doses of antibiotics and the emergence of drug-resistant bacteria. Natural hydrogels can be utilized as tissue-engineered scaffolds to imitate the microstructure of the extracellular matrix, along with many sources of raw materials and excellent biocompatibility. However, there are still some limitations to their practical applications, such as poor mechanical behavior, a narrow adjustable range of structure and performance, and easy fragmentation. Numerous studies have shown that the application of bone-defect-filling materials can be achieved either by modifying or adding various biological materials[40–42]. For instance, Wang et al.[43] endowed GelMA cryogel microspheres with strengthened mechanical properties and facilitated bone healing by introducing HA and calcium silicate fibers. Weng et al.[44] designed a MgAlEu-LDH-functionalized hydroxyapatite scaffold with enhanced osteogenic and angiogenic properties compared with pristine hydroxyapatite. *A. davidianus* has attracted extensive attention owing to its antibacterial properties, excellent toughness, and biocompatibility. Therefore, in our study, SSAD was selected as a tissue engineering scaffold. As shown in Figs. 2A and 3C, SSAD hydrogels are native materials that provide possibilities for tissue growth and nutrient transport, while possessing inherent antibacterial capabilities, which is in accordance with the results reported in previous studies. However, the pristine SSAD hydrogel has the drawbacks of poor rigidity and osteogenic effects, along with relatively limited inherent antibacterial properties.

Given the relatively low rigidity of pristine SSAD, our approach was to employ HA to increase the rigidity of the bone-defect-filling material. HA is regularly used as a bone tissue engineering material owing to its excellent rigidity and osteoconductive properties[45–48]. This superior-rigidity hydrogel was formed by thoroughly mixing equal masses of SSAD and HA. It only took approximately 10 s to form this hydrogel. As shown in Fig. 2F, G, a significantly higher storage modulus was observed for the SSAD/HA hydrogel, indicating that HA enhanced its rigidity. The microstructure and swelling rate of the SSAD/HA hydrogel also remained stable, with a slower degradation rate, helping to maintain its morphology over the long term in vivo. Thus, it provides the possibility for the long-term delivery of antibiotics in vivo to compensate for the lack of its inherent antibacterial effects.

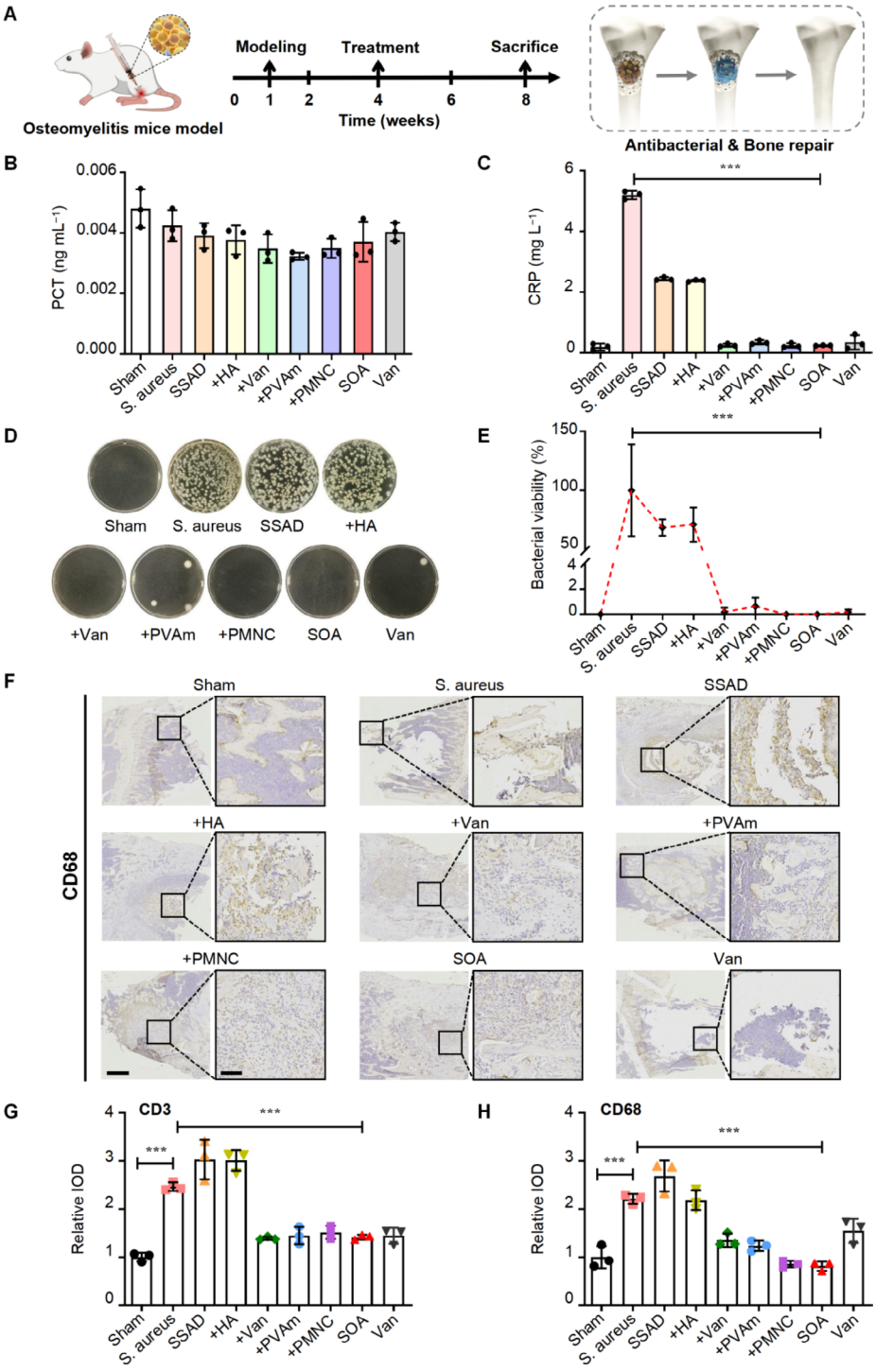

Fig. 5. Application of the SOA to treat osteomyelitis in a mouse model. **A** Schematic representation and experimental timeline for creating a mouse osteomyelitis model and SOA hydrogel treatment. **B** Blood procalcitonin (PCT) and **C** C-reactive protein (CRP) levels in mice after treatment with different hydrogels. Sham: sham *Staphylococcus aureus* model group; *S. aureus*: *S. aureus* model group; SSAD: SSAD-treated group; +HA: SSAD/HA-treated group; +Van: SSAD/HA + Van-treated group; +PVAm: SSAD/HA + Van + PVAm-treated; +PMNC: SSAD/HA + Van + PMNC-treated group; SOA: SSAD/HA + Van + PM214-treated group; Van: pure Van-treated group. **D, E** Soybean agar plates showing the antibacterial efficiency of different treatment groups against *S. aureus in vivo* and the corresponding antibacterial histograms. **F** CD68 immunohistochemical images of bone sections from each group. The **G** CD3 and **H** CD68 corresponding quantitative histograms. The black scale bar in the non-black box indicates 250 μm, and the black scale bar in the black box indicates 50 μm. All quantitative data are presented as mean values ± standard deviation ($n = 3$, * $p < 0.05$, ** $p < 0.01$, *** $p < 0.001$, ns: no significance).

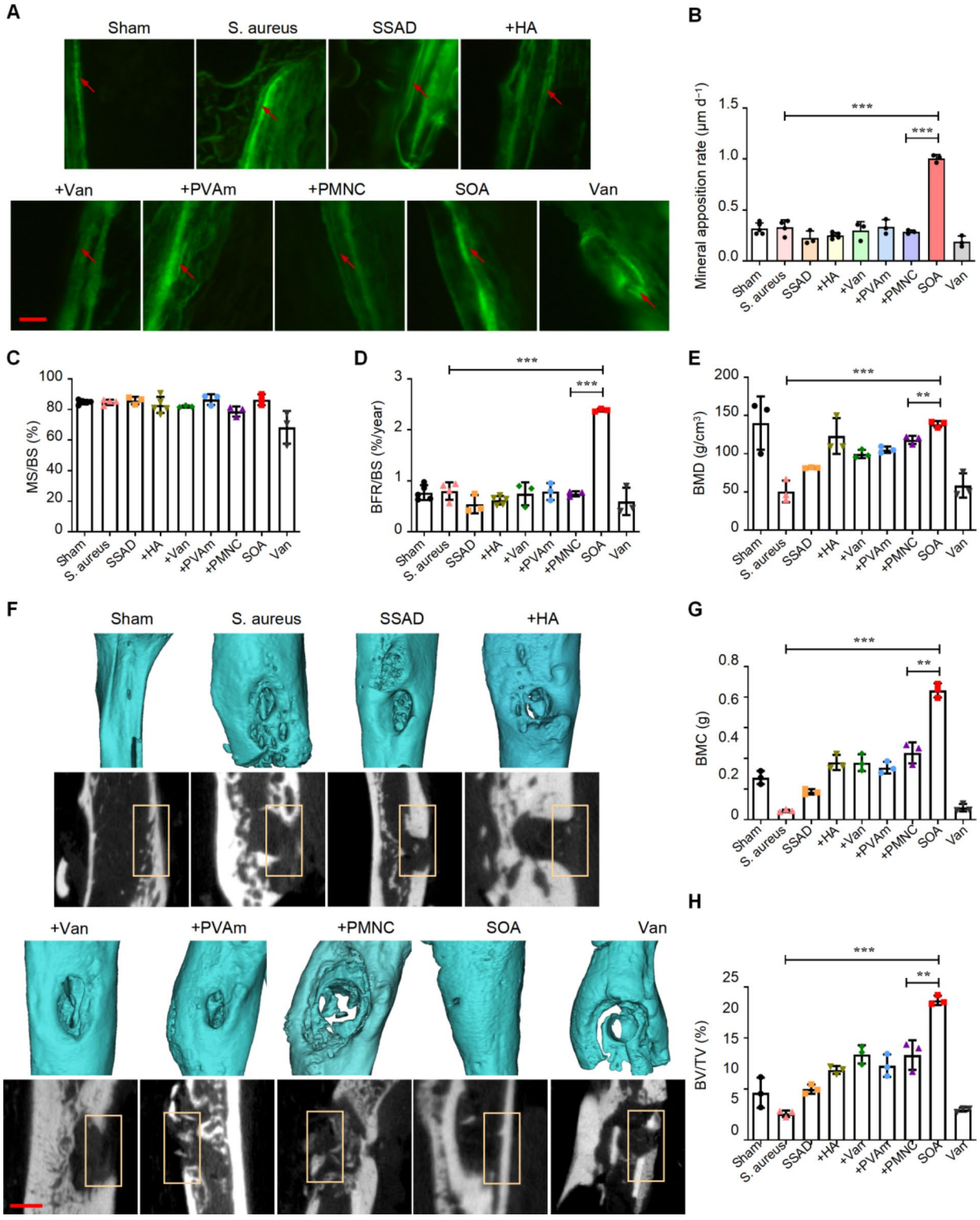

Fig. 6. Bone defect repair performance of the SOA in osteomyelitis mice. **A** Representative images showing the tibial trabecular mineral apposition rate of C57BL/6 mice in different hydrogel treatment groups. Scale bar: 10 μm. **B** Quantitative diagram of tibial trabecular mineral apposition rate in C57BL/6 mice after treatment with different hydrogels. **C** Mineralizing surface of C57BL/6 mice treated with SOA hydrogel. **D** Bone formation rate of C57BL/6 mice treated with SOA hydrogel. **E**–**H** Representative 3D reconstruction images showing microarchitecture, and microCT statistical analysis of BMD, BMC, BV/TV in proximal tibia after treatment with different hydrogels (http://www.bruker-microct.com, Version: 1.17.9.0). Scale bar: 1 mm. All quantitative data are presented as mean values ± standard deviation ($n = 3$, * $p < 0.05$, ** $p < 0.01$, *** $p < 0.001$, ns: no significance).

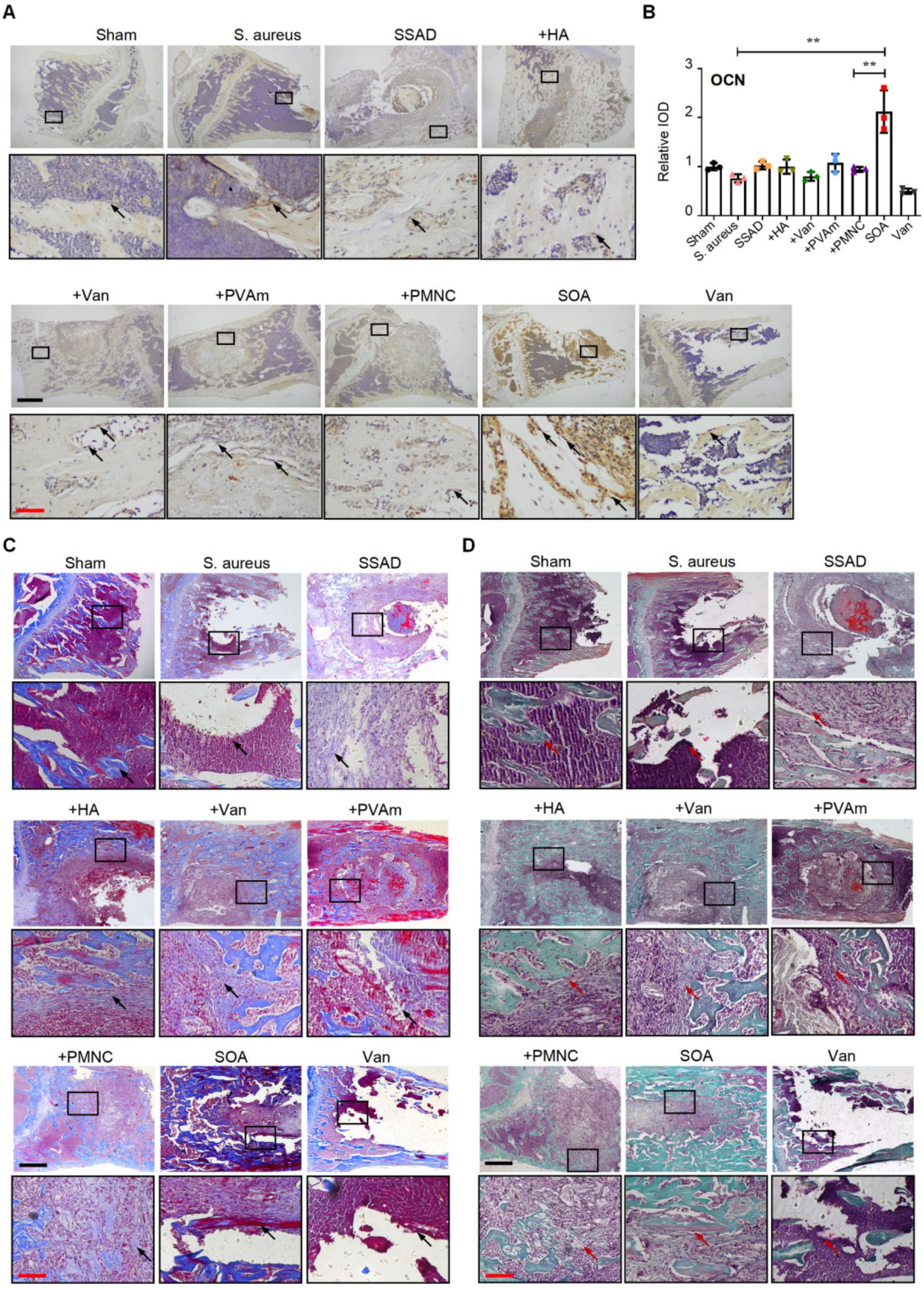

Fig. 7. Histological staining of bone repair in osteomyelitis mice. **A** Immunohistochemical images of osteocalcin (OCN) in bone sections of each group. The black scale bar indicates 500 μm, and the red scale bar in the black box indicates 50 μm. **B** Quantification of relative integrated optical density (IOD) values of OCN immunostaining using Image-Pro Plus 6.0 software (https://en.freedownloadmanager.org/users-choice/Image-pro_Plus6.0_Free_Download.html). **C** Masson's trichrome staining images of bone sections from each group (the newly formed bone is marked with a black arrow). The black scale bar indicates 500 μm, and the red scale bar in the black box indicates 50 μm. **D** Goldner's trichrome staining images of bone sections from each group (newly formed bone is marked with a red arrow). The black scale bar indicates 500 μm, and the red scale bar in the black box indicates 50 μm. All quantitative data are presented as mean values ± standard deviation ($n = 3$, * $p < 0.05$, ** $p < 0.01$, *** $p < 0.001$, ns: no significance).

As the most common causative pathogen of osteomyelitis, *S. aureus* is greatly suppressed by Van[5,49]. Boot et al.[50] reported a significant reduction in implant-associated infections after treatment with a 5% Van hydrogel in *S. aureus*-infected tibias. Therefore, Van was selected as the antibiotic for hydrogel delivery and sustained release. As shown in Fig. 3C–F, the + Van hydrogel showed antibacterial properties as efficiently as pure Van, whereas pure Van required repeated administration for osteomyelitis treatment. *S. aureus* was effectively suppressed by the Van released from SSAD/HA up to 14 d. The stable swelling rate and physical adsorption of certain noncovalent interactions may account for the long-term release of Van by SSAD/HA.

Regarding the poor osteogenic effect of the SSAD hydrogel, instead of generally adding osteogenic small-molecule drugs, we employed nucleic acid drugs. Nucleic acid drugs can directly regulate target gene expression and signaling pathways to exert therapeutic effects on diseases, and it has multiple advantages, especially in terms of high efficacy and safety[51]. Here, we combined biosynthetic recombinant RNA technology and an efficient nucleic acid delivery nanocarrier, PVAm[37,39]. Recombinant small nucleic acids (MSA) synthesized by *Escherichia coli* fermentation have excellent safety and enhanced biological activity compared with normal antagomir[36]. This MSA-based RNA therapy strategy has considerable potential for treating osteomyelitis.

The cationic polymer PVAm outperforms commercialized polyethyleneimine in terms of cost, transfection efficiency, and biosafety, and it readily coalesces with nucleic acids through electrostatic interactions, while promoting cell endocytosis. Therefore, the combination of PVAm and MSA may show better RNA delivery efficacy and prevent the premature degradation of RNA drugs by serum RNases, thereby prolonging their therapeutic effect. As illustrated in Figs. 2I and 4A-B, SSAD/HA with PVAm exhibited the sustained release of nucleic acid drugs for up to 28 d. In Fig. 4C–E, SOA showed long-term osteogenic properties, further demonstrating the efficacy of MAS-anti214 and PVAm.

SOA also exhibited an excellent serum-protective effect (Fig. 4F–G, S6). The long-term, efficient results of the SOA may be attributed to two crucial aspects. First, compared to commercial chemically synthesized nucleic acids, biosynthesized MSA-anti214 exhibits superior stability and biocompatibility, which may prevent the rapid degradation of nucleic acid drugs. Second, the positive charge held by PVAm liposomes can neutralize the negative charge of nucleic acids, forming a complex with a tight structure that aids in the slow-release of nucleic acids.

The high specificity, efficiency, and sustained effect of SOA on osteogenic differentiation and antibacterial enabled the treatment of osteomyelitis. In the osteomyelitis mouse model, SOA showed satisfactory biocompatibility (Figure S7), long-term antibacterial effect (Fig. 5), and excellent bone repair effect (Fig. 7). The new bone was found in SOA group, while only collagen fibers growth was found in other groups. During bone formation, collagen fiber was secreted and ossified to form new bone, indicating that the bone formation and bone repair rate in SOA group was faster than other groups (Fig. 7). Indicated that SOA would successfully alleviate osteomyelitis and showed promising potential as a therapeutic bone filling material for osteomyelitis.

Overall, this novel biodegradable SOA has a simplified production process, excellent safety, and highly efficient bone repair via RNA therapy. However, there are still some limitations. Detailed research has not yet been conducted on functional mechanisms such as antibacterial and bone repair. In the future, the mechanisms of action of antibiotics and nucleic acid drugs will be deeply complemented.

Conclusion

In summary, we designed and established a novel natural-polymer-based SOA hydrogel with excellent biocompatibility, slow degradation, and long-acting nucleic acid drugs and antibiotic delivery properties. Thus, the SOA not only possesses antibacterial capacity but also accelerates the repair of infectious bone defects backed by the combined effect of MSA-anti214 and preferable rigidity during osteomyelitis treatment. Therefore, this hydrogel may provide new materials for nucleic acid drug delivery for the treatment of osteomyelitis, and explore novel ideas for the treatment of other skeletal system diseases.

Materials and methods

Materials

Human mesenchymal stem cell line (hMSC) was purchased from Runde Biotechnology Co., Ltd. (Xi'an, China). PVAm was generously provided by Professor Deng Xudong of Northwestern Polytechnical University. MSA-anti214 was purchased from RQCON Biological Technology Co., Ltd. (Xi'an, China). Van (vancomycin) and 3-[4,5-dimethylthiazol-2-yl]-2,5 diphenyl tetrazolium bromide (MTT) were all obtained from Sigma Aldrich (St. Louis, MO, USA). *S. aureus* was obtained from BIO SCI (ATCC 25923; Hangzhou, China). Paraformaldehyde (4%) and collagenase II (Cls II) were purchased from BioSharps (Anhui, China). Dimethylsulfoxide (DMSO) and glycerol were obtained from BioFroxx (Guangzhou, China). Fetal bovine serum, trypsin, and Dulbecco's modified Eagle medium were purchased from Gibco (Waltham, MA, USA). HA was obtained from DULY (Nanjing, China). FAM-NC and antagomir-214 were synthesized by GenePharma (Shanghai, China). Rhodamine B was purchased from Solarbio (Beijing, China).

SSAD sample collection

SSAD samples were collected as described in a previous study[22]. Healthy adult *A. davidianus* were purchased from the Hanzhong Breeding Base in China. The purchased *A. davidianus* were kept in clean water at 16–18 °C for 1 week. Mechanical stimulation of the limbs was performed to stimulate the skin to secrete mucus. Mucus was collected in a 50 mL centrifuge tube, cleaned with deionized water, freeze-dried, ground, and stored at -20 °C.

Preparation of the SOA

The SOA consisted of SSAD, HA, PVAm, Van, and MSA-anti214. SSAD and HA (20 nm) powder were weighed proportionately in a 1:1 ratio in weight and thoroughly mixed to prepare the SSAD/HA powder.

MSA-anti214 was mixed with PVAm at a 1:1 molar ratio, and then incubated at room temperature for 10 min to prepare PM214. An equal volume of Van (100 mg/mL) was added to PM214. Mixed SSAD/HA powder was added by equal volume of the above solution to produce the SOA.

Characterization of the SOA

SEM SEM (Gemini300; ZEISS, Oberkochen, Germany) was used to characterize the micromorphology of the SSAD/HA hydrogels. The SEM images were captured at a voltage of 3 kV. The pore size was calculated using ImageJ software. The composition of the elements in the SSAD and SSAD/HA hydrogel was analyzed by EDS (EMX; HORIBA, Lyon, France).

FTIR: To evaluate changes in the chemical structure, hydrogels with various components were analyzed by FTIR (iS10; Nicolet; Thermo Fisher Scientific, Waltham, MA, USA), with a spectrum range of 400–4,000 cm^{-1}, resolution of 4 cm^{-1} and a signal-to-noise ratio of 50,000:1[52].

Rheology The rheological properties of different hydrogels were analyzed by a rheometer (MCR92; Anton Paar, Graz, Austria). The appropriate amount of hydrogel was added to the sample table with parallel plates 50 mm apart, a 1 mm gap, and a test temperature of 25 °C. Amplitude scanning was set to a shear strain range of 0.1–10%, and logarithmic take-point[52].

Water content The water content of the hydrogels was calculated using Eq. (1)[52].

$$\left(W_w - W_d\right)/W_w \times 100\% \tag{1}$$

W_w: hydrogel weight. W_d: freeze-dried hydrogel weight.

Swelling ratio The swelling ratios were calculated using Eq. (2)[53].

$$\left(W_N - W_0\right)/W_0 \times 100\% \tag{2}$$

W_0: initial hydrogel weight. W_N: water-soaked hydrogel weight.

Degradation ratio The degradation ratio was calculated using Eq. (3)[53].

$$\left(W_0 - W_N\right)/W_0 \times 100\% \tag{3}$$

W_0: initial hydrogel weight. W_N: collagenase II treated hydrogel weight.

PVAm preparation

PVAm aqueous solution (molecular weight 1100, concentration 10%) was dialyzed (molecular weight < 10,000) and filtered through a 5 μm pore size syringe. The final solution was freeze-dried to obtain the purified PVAm. Then, the powder was re-dissolved in distilled water for backup use[34].

Slow-release

The prepared hydrogel samples (Rhodamine B: 5 μg/mL, FAM-NC: 100 μM, SSAD/HA: 100 μL) were washed by deionized water for 30 min, then immersed in 200 μL deionized water and placed at 4 °C (Rhodamine B was tested at room temperature) for slow-release. After all slow-release solutions were collected at certain intervals (1 d, 2 d, 3 d, 4 d, 7 d, 14 d, 28 d), 200 μL deionized water was added again to continue the slow-release process. The slow-release solution was subsequently collected to measure the fluorescence intensity and assess the slow-release effect of the SSAD/HA hydrogels on small-molecule drugs and nucleic acid drugs.

Spread plate method

A standard strain of *S. aureus* (ATCC 25923) was selected as the bacterial model for tibial osteomyelitis. *S. aureus* was cultured as previously described[54]. In brief, *S. aureus* preserved in glycerol was added in 3% tryptone soy broth (TSB; Solarbio, Beijing, China) and cultured to the logarithmic growth stage at a constant temperature of 37 ℃ and 100 rpm. The absorbance at 600 nm was adjusted to 0.36 using TSB, and the concentration of *S. aureus* was 5.4×10^7 colony-forming units (CFUs) mL^{-1}. The prepared *S. aureus* bacterial solution was mixed with different hydrogels for 1 h. The samples were diluted 1,000-fold with TSB and evenly coated onto a soybean agar plate. Then, the CFUs were counted after incubation for 12 h.

Cell culture and cytotoxicity assay

hMSCs were cultured in Dulbecco's Modified Eagle Medium, High Glucose (DMEM, KeyGEN BioTECH, KGM12800-500, Nanjing, China) containing 10% Fetal Bovine Serum (FBS, OPCEL, BS-1101, Hohhot, Inner Mongolia) and 1% penicillin and streptomycin (Penicillin-Streptomycin 10,000 U/mL, 15140122, Gibco, Carlsbad, USA). For osteogenic differentiation treatment, cells at a density of 100% were induced by osteogenic medium with DMEM, 10% FBS, 1% β-glycerophosphate (Sigma, G9422), 1% ascorbic acid (Sigma, A7631) and 1% L-glutamine. Cells were incubated at 37 °C, 5% CO_2. The treatment of SOA or other hydrogels was performed by attaching the hydrogel on the wall of the cell cultural plate, hydrogels were immersed in cell cultural medium

with not direct contact with the cells. For treatment of the slow-release solution, slow-release solutions collected at different intervals were diluted in cell cultural medium in a 1:10 ratio, and cells were cultured in the medium. The cytotoxicity of the SOA hydrogel was evaluated using the MTT assay as previously described[52].

Flow cytometry

hMSC were cultured with hydrogels for 48 h and digested by trypsin. The digested cells were fixed by 70% ice-cold ethanol. Cells were then washed and stained with 0.1 mg/mL PI solution. Cell cycle was determined by flow cytometer (FACSCalibur, BD Biosciences, USA)[55].

Cell adhesion analysis

GFP-labeled hMSC were digested, and then suspended with cell cultural medium containing 2% matrigel (v/v, Corning, 354480, NY, USA). SOA was supplemented into the cell suspension and incubated at 37 °C for 72 h. Incubated SOA was washed by PBS 5 times and then observed using a laser confocal microscope (FV3000, OLYMPUS, Japan).

Osteogenic differentiation analyses

RT-PCR, ALP staining and ARS staining were performed to evaluate the osteogenic differentiation of hMSC as previously described. RT-PCR primers were synthesized by Sangon, Inc. (Shanghai, China; Supplementary Table S1)[56].

Hemolysis assay

Fresh anticoagulated blood of mice was collected for hemolysis assay. Blood samples were centrifuged to obtain a pure erythrocyte precipitate. Subsequently, erythrocyte precipitate was suspended with PBS. Different hydrogel complexes were added to the erythrocyte suspension and maintained at 37 °C for 4.5 h. Then the supernatant was photographed and absorbance was measured with a microplate reader[54].

Establishment of tibial osteomyelitis model in mice

Ninety 2-month-old male C57BL/6 mice (25 ± 5 *g*) were purchased from Huafukang Bioscience Co., Ltd. (Beijing, China) and were treated as previously described[57]. Euthanasia was performed with CO_2. All animal care and experimental procedures were approved by the Ethics Committee of North Sichuan Medical College. Efforts were made to minimize the number of mice used and their suffering in all animal procedures.

Therapeutic hydrogels in mice with osteomyelitis

Three weeks after tibial osteomyelitis model established, a 1.2 mm borehole was created at the tibial osteomyelitis site using a dental drill[57]. The osteomyelitis area was thoroughly washed with sterile PBS, and different hydrogels were implanted into the bone defect. The mice were sacrificed after being kept for 4 weeks. Blood samples were collected for the determination of inflammatory indicators CRP and PCT using an Axceed 360 chemiluminescent immunoassay (Bioscience, Tianjin, China). Tibia samples were collected for spread plate, bone histomorphometric analyses, and Immunohistochemistry (IHC) staining.

Blood chemical analysis and H&E staining

Blood chemical analysis and H&E staining were performed to assess the biocompatibility of the hydrogels in vivo. The blood supernatants were isolated for AST, ALT, BUN, and Cr analysis using an ADVIA 2400 chemistry system (Siemens Healthcare Diagnostics, Tarrytown, NY, USA).

Heart, liver, spleen, lung, and kidney samples were collected, fixed, and paraffin sections were made for H&E staining. Histological images were obtained using an optical microscope.

Bone histomorphometric analyses

The effect of SOA hydrogel on bone formation was investigated using bone histomorphometric analyses. Double calcein labeling was performed as previously described[58,59] Paraffin sections were subjected to Masson's trichrome staining (MTS) and Goldner's trichrome staining (GTS) to detect new bone growth using standard protocols.

Microstructure of mice tibia was performed by the microCT system (version 6.5, viva CT40, SCANCO Medical, Switzerland) and the proximal tibia metaphysis was analyzed. Images were reconstructed and calibrated at the isotropic voxel size of 10.5 mm, respectively (70 kVp, 114 mA, 200 ms integration time, 260 thresholds, 1200 mg HA/cm^3). Using the Scanco evaluation software, regions of interest (ROIs) were defined for the bone defect region of tibia. The entire tibia was reoriented with the middiaphysis parallel to the z-axis. The bone defect region was analyzed by manually contouring for three-dimensional reconstruction (sigma = 1.2, supports = 2 and threshold = 200) to calculate the following parameters including bone mineral density (BMD), bone volume to tissue volume (BV/TV) and bone mineral content (BMC), for bone microarchitecture[60].

Immunohistochemistry

Immunohistochemistry (IHC) staining was performed to determine the protein levels of the inflammatory markers, CD3 (Mouse mAb, 1:100, Santa Cruz Biotech, sc-20047, Dallas, TX) and CD68 (Mouse mAb, 1:100, Santa Cruz Biotech, sc-20060, Dallas, TX), and the bone-specific marker, OCN (Mouse mAb, 1:200, Santa Cruz Biotech, sc-73464, Dallas, TX), as previously described[58].

Statistical analyses

The data are presented as the mean value ± standard deviation and were analyzed using Prism 9.4 (GraphPad Software, La Jolla, CA, USA) via Student's *t*-test and one-way analysis of variance. All experiments were performed on three independent occasions. $p < 0.05$ was regarded as significantly different.

Data availability

The datasets used and/or analysed during the current study available from the corresponding author on reasonable request.

Received: 2 May 2024; Accepted: 9 October 2024
Published online: 19 October 2024

References

1. Foster, A. L. et al. Fracture-related infection: current methods for prevention and treatment. *Expert Rev. Anti. Infect. Ther.* **18**, 307 (2020).
2. Depypere, M. et al. Pathogenesis and management of fracture-related infection. *Clin. Microbiol. Infect.* **26**, 572 (2020).
3. Dirschl, D. R. & Almekinders, L. C. Osteomyelitis. Common causes and treatment recommendations. *Drugs*. **45**, 29 (1993).
4. Wang, X. et al. Current data on extremities chronic osteomyelitis in southwest China: epidemiology, microbiology and therapeutic consequences. *Sci. Rep. UK*. **7**, 16251 (2017).
5. Kavanagh, N. et al. Staphylococcal osteomyelitis: disease progression, treatment challenges, and future directions. *Clin. Microbiol. Rev.* **31**, e00084-17 (2018).
6. Darouiche, R. O. Treatment of infections associated with surgical implants. *New. Engl. J. Med.* **350**, 1422 (2004).
7. Rao, N., Ziran, B. H. & Lipsky, B. A. Treating osteomyelitis: antibiotics and surgery. *Plast. Reconstr. Surg.* **127**(Suppl 1), 177S (2011).
8. Krajewski, J. et al. Successful treatment of extensively drug-resistant *Pseudomonas aeruginosa* osteomyelitis using a colistin- and tobramycin-impregnated PMMA spacer. *Int. J. Antimicrob. Agents* **44**, 363 (2014).
9. Mistry, S. et al. Treatment of long bone infection by a biodegradable bone cement releasing antibiotics in human. *J. Control Release* **346**, 180 (2022).
10. Cao, Z., Jiang, D., Yan, L. & Wu, J. In vitro and in vivo drug release and antibacterial properties of the novel Vancomycin-loaded bone-like hydroxyapatite/poly amino acid scaffold. *Int. J. Nanomed.* **12**, 1841 (2017).
11. Feng, Y., Guo, W., Hu, L., Yi, X. & Tang, F. Application of hydrogels as sustained-release drug carriers in bone defect repair. *Polymers (Basel)* **14**, 4906 (2022).
12. Liu, Y., Li, X. & Liang, A. Current research progress of local drug delivery systems based on biodegradable polymers in treating chronic osteomyelitis. *Front. Bioeng. Biotech.* **10**, 1042128 (2022).
13. Tan, H. et al. The use of quaternised chitosan-loaded PMMA to inhibit biofilm formation and downregulate the virulence-associated gene expression of antibiotic-resistant staphylococcus. *Biomaterials* **33**, 365 (2012).
14. Inzana, J. A., Schwarz, E. M., Kates, S. L. & Awad, H. A. Biomaterials approaches to treating implant-associated osteomyelitis. *Biomaterials* **81**, 58 (2016).
15. Pupillo, D. et al. Enhancing biocompatibility and antibacterial activity of Ti_6Al_4V by entrapping Ag and hydroxyapatite inside alginate filled pores of TiO_2 layer grown by spark anodizing. *Adv. Mater. Interfaces.* **10**, e2201725 (2023).
16. Yi, S. et al. Flat silk cocoon-based dressing: daylight-driven rechargeable antibacterial membranes accelerate infected wound healing. *Adv. Healthc. Mater.* **11**, e2201397 (2022).
17. Xu, Z., Wu, M., Gao, W., & Bai, H. A transparent skin-inspired composite film with outstanding tear resistance based on flat silk cocoon. *Adv. Mater.* **32**, e2002695 (2020).
18. Changez, M., Koul, V. & Dinda, A. K. Efficacy of antibiotics-loaded interpenetrating network (IPNs) hydrogel based on poly(acrylic acid) and gelatin for treatment of experimental osteomyelitis: in vivo study. *Biomaterials* **26**, 2095 (2005).
19. Yan, Y. et al. Enhanced osteogenesis of bone marrow-derived mesenchymal stem cells by a functionalized silk fibroin hydrogel for bone defect repair. *Adv. Healthc. Mater.* **8**, e1801043 (2019).
20. Nilforoushzadeh, M. A. et al. Combination therapy of trichloroacetic acid, human autologous fibroblast injection and fibroblast seeded microfibrous collagen scaffold as a novel treatment for osteomyelitis diabetic foot ulcer. *J. Diabetes Invest.* **12**, 1112 (2021).
21. Xie, X. et al. A self-assembled bilayer polypeptide-engineered hydrogel for spatiotemporal modulation of bactericidal and anti-inflammation process in osteomyelitis treatment. *J. Nanobiotechnol.* **20**, 416 (2022).
22. Deng, J. et al. A bioinspired medical adhesive derived from skin secretion of *Andrias davidianus* for wound healing. *Adv. Funct. Mater.* **29**, 1809110 (2019).
23. Zhang, X. M. et al. A bioinspired hemostatic powder derived from the skin secretion of Andrias davidianus for rapid hemostasis and intraoral wound healing.*Small* **18**, e2101699 (2022).
24. Liu, X. et al. Bioinspired *Andrias davidianus*-derived wound dressings for localized drug-elution. *Bioact Mater.* **15**, 482 (2022).
25. Dang, R. et al. A natural hydrogel with prohealing properties enhances tendon regeneration. *Small*. **18**, e2105255 (2022).
26. Unnikrishnan, V. et al. Cellular and sub-chronic toxicity of hydroxyapatite porous beads loaded with antibiotic in rabbits, indented for chronic osteomyelitis. *Int. J. Pharmaceut*. **616**, 121535 (2022).
27. Shi, Z. et al. Nanohydroxyapatite, nanosilicate-reinforced injectable, and biomimetic gelatin-methacryloyl hydrogel for bone tissue engineering. *Int. J. Nanomed*. **16**, 5603 (2021). Nanohydroxyapatite, Nanosilicate-Reinforced.
28. Kumar, G. S., Govindan, R. & Girija, E. K. In situ synthesis, characterization and in vitro studies of ciprofloxacin loaded hydroxyapatite nanoparticles for the treatment of osteomyelitis. *J. Mater. Chem. B* **2**, 5052 (2014).
29. Tao, J. et al. Injectable chitosan-based thermosensitive hydrogel/nanoparticle-loaded system for local delivery of Vancomycin in the treatment of osteomyelitis. *Int. J. Nanomed.* **15**, 5855 (2020).
30. Sun, C. K. et al. Transglutaminase cross-linked gelatin-alginate-antibacterial hydrogel as the drug delivery-coatings for implant-related infections. *Polymers (Basel)* **13**, 414 (2021).
31. Rastegar, A., Mahmoodi, M., Mirjalili, M. & Nasirizadeh, N. Platelet-rich fibrin-loaded PCL/chitosan core-shell fibers scaffold for enhanced osteogenic differentiation of mesenchymal stem cells. *Carbohydr. Polym.* **269**, 118351 (2021).
32. Tan, X., Jia, F., Wang, P. & Zhang, K. Nucleic acid-based drug delivery strategies. *J. Control Release*. **323**, 240 (2020).
33. Afonin, K. A., Dobrovolskaia, M. A., Church, G. & Bathe, M. Opportunities, barriers, and a strategy for overcoming translational challenges to therapeutic nucleic acid nanotechnology. *ACS Nano*. **14**, 9221 (2020).
34. Tian, Y. et al. Polyvinylamine with moderate binding affinity as a highly effective vehicle for RNA delivery. *J. Control Release* **345**, 20 (2022).
35. Wang, X. et al. miR-214 targets ATF4 to inhibit bone formation. *Nat. Med.* **19**, 93 (2013).
36. Yin, C. et al. Mir-129-5p inhibits bone formation through TCF4. *Front. Cell. Dev. Biol.* **8**, 600641 (2020).
37. Li, X. et al. Bioengineered miR-27b-3p and mir-328-3p modulate drug metabolism and disposition via the regulation of target ADME gene expression. *Acta Pharm. Sin. B* **9**, 639 (2019).
38. Dowdy, S. F. Overcoming cellular barriers for RNA therapeutics. *Nat. Biotechnol.* **35**, 222 (2017).

39. Ho, P. Y. et al. Bioengineered noncoding RNAs selectively change Cellular miRNome profiles for cancer therapy. *J. Pharmacol. Exp. Ther.* **365**, 494 (2018).
40. Zhang, S. X. et al. Osteogenic and anti-inflammatory potential of oligochitosan nanoparticles in treating osteomyelitis. *Biomater. Adv.* **135**, 112681 (2022).
41. Liu, X. et al. A functionalized collagen-I scaffold delivers microRNA 21-loaded exosomes for spinal cord injury repair. *Acta Biomater.* **154**, 385 (2022).
42. Boot, W. et al. A hyaluronic acid hydrogel loaded with gentamicin and vancomycin successfully eradicates chronic methicillin-resistant staphylococcus aureus orthopedic infection in a sheep model. *Antimicrob. Agents Chemother*. **65**, e01840-20, (2021).
43. Wang, Y. et al. Injectable, high specific surface area cryogel microscaffolds integrated with osteoinductive bioceramic fibers for enhanced bone regeneration. *ACS Appl. Mater. Inter.* **15**, 20661 (2023).
44. Wang, G. et al. Surface functionalization of hydroxyapatite scaffolds with MgAlEu-LDH nanosheets for high-performance bone regeneration. *Adv. Sci.* **10**, e2204234 (2022).
45. Zhou, H. & Lee, J. Nanoscale hydroxyapatite particles for bone tissue engineering. *Acta Biomater.* **7**, 2769 (2011).
46. Tavakoli-darestani, R., Manafi-rasi, A. & Kamrani-rad, A. Dexamethasone-loaded hydroxyapatite enhances bone regeneration in rat calvarial defects. *Mol. Biol. Rep.* **41**, 423 (2014).
47. Kuang, Z. et al. Osteogenic and antibacterial dual functions of a novel levofloxacin loaded mesoporous silica microspheres/nano-hydroxyapatite/polyurethane composite scaffold. *Genes Dis.* **8**, 193 (2021).
48. Benedini, L., Laiuppa, J., Santillan, G., Baldini, M. & Messina, P. Antibacterial alginate/nano-hydroxyapatite composites for bone tissue engineering: assessment of their bioactivity, biocompatibility, and antibacterial activity. *Mater. Sci. Eng. C Mater*. **115**, 111101 (2020).
49. Wilhelm, M. P. Vancomycin *Mayo Clin. Proc*. **66**, 1165 (1991).
50. Boot, W. et al. Prophylaxis of implant-related infections by local release of Vancomycin from a hydrogel in rabbits. *Eur. Cells Mater.* **39**, 108 (2020).
51. Gupta, A. et al. Nucleic acid delivery for therapeutic applications. *Drug Deliv Rev.* **178**, 113834 (2021).
52. Motasadizadeh, H. et al. Dual drug delivery system of teicoplanin and phenamil based on pH-sensitive silk fibroin/sodium alginate hydrogel scaffold for treating chronic bone infection. *Biomater. Adv.* **139**, 213032 (2022).
53. Zhao, L. et al. A novel smart injectable hydrogel prepared by microbial transglutaminase and human-like collagen: its characterization and biocompatibility. *Mater. Sci. Eng. C Mater.* **68**, 317 (2016).
54. Liu, G. et al. Polydopamine nanosheets doped injectable hydrogel with nitric oxide release and photothermal effects for bacterial ablation and wound healing. *Adv. Healthc. Mater.* **23**, e2101476 (2021).
55. Hu, L. et al. Knockdown of microtubule actin crosslinking factor 1 inhibits cell proliferation in MC3T3-E1 osteoblastic cells. *BMB Rep.* **48**, 583 (2015).
56. Yin, C. et al. Long noncoding RNA AK039312 and AK079370 inhibits bone formation via miR-199b-5p. *Pharmacol. Res.* **163**, 105230 (2021).
57. Li, K. et al. PD-1/PD-L1 blockade is a potent adjuvant in treatment of *Staphylococcus aureus* osteomyelitis in mice. *Mol. Ther.* **31**, 174 (2023).
58. Yin, C. et al. A novel long noncoding RNA AK016739 inhibits osteoblast differentiation and bone formation. *J. Cell. Physiol.* **234**, 11524 (2019).
59. Ushiku, C. et al. Long bone fracture repair in mice harboring GFP reporters for cells within the osteoblastic lineage. *J. Orthop. Res.* **28**, 1338 (2010).
60. Yin, C. et al. MACF1 alleviates aging-related osteoporosis via HES1. *J. Cell. Mol. Med.* **25**, 6242 (2021).

Acknowledgements

This work was supported by the National Natural Science Foundation of China (82272436, 32000924), Sichuan Science and Technology Program (23NSFSC6012), Medical Science and Technology Project of the Health Planning Committee of Sichuan (21PJ101), Doctor Foundation of North Sichuan Medical College (CBY19-QD01), "Take the Lead" Program of Affiliated Hospital of North Sichuan Medical College (2022JB007), Clinical Research Program of Affiliated Hospital of North Sichuan Medical College (2021LC008), Sichuan Science and Technology Innovation Seed Project (MZGC20230044), and Sichuan Science and Technology Program (2022NSFSC1554).

Author contributions

Conceptualization, C.Y. and M.D.; Data curation, C.Y., M.D. and J. Y.; Formal analysis, C.Y. and M.D.; Funding acquisition, C.Y. and B.G.; Investigation, C.Y., M.D., J.Y., Y.C., K.Z., Y.H. and Y.M.; Methodology, C.Y., M.D., Y.T. and B.Z.; Project administration, C.Y. and M.D.; Resources, C.Y., X.D., X.G. and B.G.; Supervision, C.Y., M.D., X.D., X.G. and B.G.; Validation, C.Y. and M.D.; Visualization, C.Y. and M.D.; Writing–original draft, C.Y., M.D., Y.C. and B.G.; Writing–review & editing, C.Y., M.D., Y.C. and B.G.

Declarations

Competing interests

The authors declare no competing interests.

Ethics declarations

The study was conducted according to the ARRIVE guidelines, and approved by the Ethics Committee of North Sichuan Medical College (protocol code 2023078 and date 2023Y 09 M 05D of approval). We confirm that all methods were performed in accordance with the relevant guidelines and regulations.

Additional information

Supplementary Information The online version contains supplementary material available at https://doi.org/10.1038/s41598-024-75997-8.

Correspondence and requests for materials should be addressed to X.G. or B.G.